Process Safety and Environmental Protection 164 (2022) 517–527

Contents lists available at ScienceDirect

Process Safety and Environmental Protection

journal homepage: www.journals.elsevier.com/process-safety-and-environmental-protection

Experimentally exploring thermal runaway propagation and prevention in the prismatic lithium-ion battery with different connections

Zhizuan Zhou [a,b], Xiaodong Zhou [a], Boxuan Wang [a], K.M. Liew [b,*], Lizhong Yang [a,*]

[a] State Key Laboratory of Fire Science, University of Science and Technology of China, Hefei, Anhui 230026, China
[b] Department of Architecture and Civil Engineering, City University of Hong Kong, Kowloon, Hong Kong, China

ARTICLE INFO

Keywords:
Thermal runaway propagation
Lithium-ion battery
Propagation prevention
Heat transfer

ABSTRACT

Thermal runaway (TR) propagation is a critical challenge in the safety application of lithium-ion batteries (LIBs). In this study, the battery modules with different connection modes are designed to reveal TR propagation mechanisms, and a passive strategy based on thermal insulation is proposed to inhibit TR propagation. The temperature, voltage, heat transfer of battery module, as well as the equivalent flux power during TR propagation are captured and analyzed. The batteries in parallel experience fiercer combustion and propagation in comparison with the batteries without connection, which is because the parallel connection mode intensifies the exothermic reactions inside the battery. Particularly, the energy from the former battery contributes to the dominant heat source for triggering TR of its adjacent battery, accounting for 52 %– 67 %. Compared to the module without connection, the module in parallel releases much higher heat flux to adjacent batteries, leading to shorter TR propagation time and severer TR propagation. Furthermore, the aerogel can completely prevent TR propagations with different connection modes. The average flux power of the former battery to its neighboring battery can be reduced from 400 W to 35 W by inserting aerogel. The results provide new insights into TR propagation mechanism and its prevention, which are beneficial to the safety design of battery modules.

1. Introduction

Global warming continues to intensify due to the massive emission of greenhouse gases in recent years (Ma et al., 2021; Rogelj et al., 2016), which has attracted worldwide attention. To alleviate the issue, numerous clean energy resources and low-carbon energy technologies are proposed and adopted. Lithium-ion battery (LIB), which is considered as one of the most promising technologies to relieve carbon emissions (Zhou et al., 2022a), are widely used in consumer electronics, electric transport and energy storage systems (Niu et al., 2019; Xu et al., 2019). Owing to its high energy density, non-memory effect and environmental friendliness (Feng et al., 2019; Li et al., 2018; Mao et al., 2020; Zhou et al., 2022b), LIB plays an increasingly important role in our society. However, safety accidents involving thermal runaway (TR) occurred occasionally (Feng et al., 2020; Wang et al., 2019), bringing a great barrier to the widespread application of LIBs. As the core of the safety issue for LIBs, TR have aroused greater concerns (Lisbona and Snee, 2011). TR can be triggered when LIBs are exposed to extreme conditions because of the application of active electrodes and organic solvent (Chen et al., 2019; Liu et al., 2020; Ping et al., 2015). Once TR is induced, a large amount of heat and flammable gases will be released by LIBs (Duh et al., 2020; Lyon and Walters, 2016), exhibiting a huge risk of fire or explosion.

The TR, originating from a single LIB, will propagate to the neighboring batteries due to the tight contact between battery shells (Kriston et al., 2020), resulting in TR propagation within the battery module. Under TR propagation, the heat released from the battery module is enormous and may cause catastrophic disasters (Ping et al., 2018). Additionally, the tremendous gases released by batteries during TR propagation are flammable and toxic (Larsson et al., 2018; Yuan et al., 2020), which are harmful to humankind and the environment. Therefore, many efforts have been implemented to solve the challenge. For example, Chen et al. (2020) quantitatively analyzed the fire hazards of TR propagation through full-scale burning tests. Said et al. (2020), (2019) revealed that the total heats generated normalized by the electrical energy stored are 3.5, 2.9 and 2.5 for lithium cobalt oxide (LCO), lithium nickel manganese cobalt oxide (NMC) and lithium iron phosphate (LFP) batteries through experimental approaches. Huang et al. (2021a) found that LFP battery modules is much safer than NMC battery modules in terms of combustion behavior and TR propagation time.

In order to meet the voltage and capacity demands, multiple

* Corresponding authors.
E-mail addresses: kmliew@cityu.edu.hk (K.M. Liew), yanglz@ustc.edu.cn (L. Yang).

https://doi.org/10.1016/j.psep.2022.06.048
Received 8 May 2022; Received in revised form 21 June 2022; Accepted 21 June 2022
Available online 23 June 2022

Nomenclature

$T_{max,i}$	Maximum temperature of battery i, ℃.
$T_{onset,i}$	Onset temperature of TR for battery i, ℃.
T_b	Average temperature of battery, ℃.
T_∞	Ambient temperature, ℃.
Q_{total}	Internal heat increasing in battery, kJ.
Q_b	The heat absorbed by battery, kJ.
Q_{self}	Self-generated heat of battery, kJ.
$Q_{b,i}$	Heat absorbed by battery i, kJ.
$Q_{b-j,i}$	Contribution of the heat generated from battery j to induce TR of battery i, kJ.
$Q_{heater,i}$	Contribution of the heat transferred from the heater to induce TR of battery i, kJ.
P_{ave}	Average heat flux, W.
m_b	Mass of battery, g.
c_b	Specific heat of battery, $kJ \bullet kg^{-1} \bullet K^{-1}$.
V	Terminal voltage of battery module, V.
E	Electric potential of battery, V.
I	Current transferred, A.
Q_e	Transfer capacity of electricity, Ah.
H_e	Energy of transferred electricity, kJ.
N	Number of normal batteries.
R_b	Resistance of normal battery, mΩ.
R_{TR}	Resistance of TR battery, mΩ.

Acronyms

LIB	Lithium-ion battery.
SOC	State of charge.
LFP	Lithium iron phosphate.

batteries are assembled into a battery system with different electrical connections. The abovementioned efforts all focused on TR propagation of the battery modules without connection. Similarly, TR propagation characteristics of the battery module in series have also been investigated by numerous scholars (Feng et al., 2015b; Huang et al., 2016; Zhong et al., 2018), which are similar to that of the module without connection (Huang et al., 2020). Compared with the battery module without electrical connection or in series, a fiercer TR behavior and severer TR propagation can be observed in the battery module in parallel (Lamb et al., 2015; Wilke et al., 2017), and the TR propagation is always accompanied with the electricity transfer due to the parallel connection mode. Gao et al. (2019) estimated the transferred electricity and predicted the Joule heat generation by using an equivalent circuit model. Xu et al. (2021a) investigated the hazards of electricity transfer in modules with hybrid electrical connections, and reveal the transferred electricity has a slight influence on TR propagation. For the battery module without electrical connection or in series, the dominant heat transfer during TR propagation is the thermal conduction between battery shells (Feng et al., 2015b; Huang et al., 2021b). However, the knowledge about heat transfer mechanism of the module in parallel is limited due to the presence of electricity transfer, and the cause of the fiercer TR behavior and severer TR propagation in the battery module in parallel is still unclear.

In addition to the studies on the characteristics and mechanisms of TR propagation, a lot of researchers concerned on developing effective strategies to prevent or alleviate TR propagation, including the passive protection strategies (Qin et al., 2021; Wu et al., 2020; Xu et al., 2021b) and the active protection strategies (Feng et al., 2015a; Lee et al., 2020; Yuan et al., 2019). Liu and Said et al. revealed that water mist has excellent performance in suppressing TR propagation of 18650 lithium-ion cells through experiments (Liu et al., 2020; Said et al., 2021). Zhao et al. compared the inhibiting effects of different fire extinguishing agents (ABC ultrafine dry powder, BC ultrafine dry powder and Novec 1230) on TR propagation of 18650 cells, and found that Novec 1230 has the best performance in inhibiting fire (Zhao et al., 2021). However, the strategies by adopting water mist or fire extinguishing agent is only suitable for the battery with small energy capacity. Once TR propagation occurs in the large-format battery module, enormous heat will release, causing the agent is insufficient to suppress the propagation. And the consumption of the fire extinguishing agent is huge for inhibiting the TR propagation of the battery with large energy capacity. Actually, heat transfer is considered to be the reason of resulting in TR of the adjacent batteries (Zhao et al., 2021), and thermal insulation is currently regarded as the countermeasure to TR propagation (Li et al., 2021). Consequently, a few studies have adopted thermal insulation materials to inhibit TR propagation. Lee et al. (2020) compared the effectiveness of several passive mitigation strategies for 18650 battery modules, which include implementing 5 mm gaps and inserting physical barriers. Niu et al. (2022) used the ultra-light plates based on hollow glass microspheres as firewalls to inhibit TR propagation of the batteries without connection, and found the 3-mm plate can completely prevent TR propagation. However, previous studies only focused on the passive suppression strategies of the battery module without connection or in series, little attention has been paid to the prevention of TR propagation for the battery module in parallel, especially for the large-format battery module. The battery module in parallel suffers from more severe TR behavior and propagation in comparison with other electrical connections, exhibiting higher risk of fire or explosion. Therefore, an investigation on suppressing TR propagation of the battery module in parallel is urgently needed to meet the increasing demands of thermally safer battery modules.

In this work, a series of experiments are carried out to investigate TR propagation and its prevention of prismatic battery modules with different electrical connections. The TR propagation characteristics are analyzed in detail from the perspective of temperature, voltage, mass loss, heat transfer, as well as heat flux. An effective prevent strategy with the thermal insulation is proposed to inhibit TR propagation of the battery module in parallel. The aim of this work is to address knowledge gaps in the literature with regard to the TR propagation behavior and its prevention of LFP battery modules with different connection modes. The objectives of this work are as follows: (1) to implement a comprehensive analysis of prismatic LFP battery to enhance the understanding of TR propagation characteristics under varying connection modes; (2) to identify the heat transfer and the equivalent flux power between adjacent batteries during TR propagation, providing essential information for the prevention of TR propagation; (3) reveal the primary cause of the severer TR propagation behaviors in the battery module in parallel; (4) quantify the inhibited effects of the thermal insulation on TR propagation of battery modules with different connection modes, providing sufficient reference for the safety design of prismatic battery module.

2. Materials and methods

2.1. The samples

A commercial prismatic battery manufactured by EVE Energy Co. Ltd is investigated in this work, whose electrodes are $LiFePO_4$ and graphite. The battery is used in electric vehicles and energy storage systems, with a capacity of 50 Ah and a nominal voltage of 3.2 V. The physical dimensions of this battery are 29 mm in thickness, 135 mm in length, and 180 mm in height. The mass of the battery without plastic packaging is 1395 ± 5.0 g. Prior to TR propagation tests, the capacity of the battery is characterized by using a cycler (NEWARE CT-4004–10V100A-NFA) under constant current (50 A) discharging and constant current (50 A)-

constant voltage (3.65 V, 0.5 A cut-off current) charging. The batteries in all TR propagation tests are charged to 100 % SOC.

As an appropriate thermal insulation material for preventing TR propagation (Yang et al., 2020), the aerogel felt with 3 mm thickness is employed in this work. The aerogel felt has a grid structure of nano-multi-space with a porosity of more than 90 %, bringing a low density (200 kg m^{-3}) and a low thermal conductivity coefficient (0.018 W m^{-1} K^{-1}).

2.2. Experimental setup

The experimental platform for TR propagation tests is illustrated in Fig. 1(a). Four prismatic batteries and a heater are tightly clamped by a steel fixture. The clamped battery module with a total capacity of 200 Ah is placed in a large combustion chamber. An electrical balance ($MSE142^{02}S–^{0}CE$) is employed to measure the mass loss during TR propagation tests. A thermal insulating layer is placed under the battery module to minimize heat leaks and protect the electrical balance. The gases and smoke released by TR batteries during the test are extracted through the smoke hood and the exhaust duct. In addition, a video camera (SONY FDR-AX40) is used to monitor the jet (combustion) behavior and TR propagation.

Battery i is used to describe the batteries within the module, and battery 1 is near the heater. Two K-type thermocouples with a diameter of 1 mm (recorded at a frequency of 1 Hz) are attached to the front and back surfaces of each battery within the battery module to measure its temperature variations, as illustrated in Fig. 1(b). The front and back surfaces of battery i are reflected by T_{i-f} and T_{i-b}. The Kapton tape is used to fix the thermocouples on the surfaces of each battery, which can keep the close contact between thermocouples and the battery surface. The temperatures and voltage of each battery are recorded by the equipment of ICPCON I-7018 and I-7017 with a frequency of 1 Hz.

2.3. Experimental design

Two types of battery modules are designed to investigate the effects of different connections on TR propagation, as shown in Fig. 1(c) – (d). The four batteries within the module are surrounded by thermal insulating layers (ceramic fiberboard) to minimize the heat leak from the module to the environment. A heater made of copper with 500 W heating power is used to trigger battery 1 to experience TR initially. The heater will be immediately turned off once TR of battery 1 is captured. For module 1, there is no connection mode for batteries. For the module 2, the four batteries are connected in parallel using copper connectors with a thickness of 1 mm. In addition, two kinds of battery modules are proposed to study the preventing performances of aerogel on TR propagation of module 1 and 2. As shown in Fig. 1(e) - (f), aerogel felts with the same size as the surface of the battery are inserted between adjacent batteries to enhance the thermal resistance in the direction of battery thickness for module 3 and 4. In this work, four groups of TR propagation tests under different settings are implemented to reveal the TR propagation characteristics and its preventing mechanism of different connections, as listed in Table 1.

3. Results

3.1. TR propagation characteristics with different connections

3.1.1. TR propagation phenomena

The TR behaviors of batteries within module 1 and 2 are presented in Fig. 2. During TR propagation, only decomposed electrolytes and irritant gases with milk-white are ejected from the safety vent of batteries in the module without connection, whereas violent flame jets can be observed for the module in parallel. As shown in Fig. 2(a), the TR processes of each battery within the module without connection consist of four stages: safety venting, transition, jet flow and abatement. The gases and electrolyte vapors generated by thermochemical reactions accumulate inside a battery when the battery is heated, leading to an increase in the internal pressure of the battery. Once the internal pressure exceeds the threshold, the safety vent is opened to eject the gases and electrolyte vapors with high speeds, which corresponds to safety venting. During the transition, a few gases and vapors are released with slow speed (Zhou et al., 2021). When TR occurs in the battery, a violent and strong jet flow can be observed. After TR, the flow starts to abate and the jet behavior of the subsequent battery will be induced.

In contrast to TR processes of the module without connection, the module in parallel experiences jet phenomenon and combustion during TR propagation. As shown in Fig. 2(b), the behavior of safety venting of

Table 1
Experimental settings for TR propagation tests.

Test No.	Battery module	Electrical connection	Passive prevention
#1	Module 1	Without connection	No
#2	Module 2	In parallel	No
#3	Module 3	Without connection	Yes
#4	Module 4	In parallel	Yes

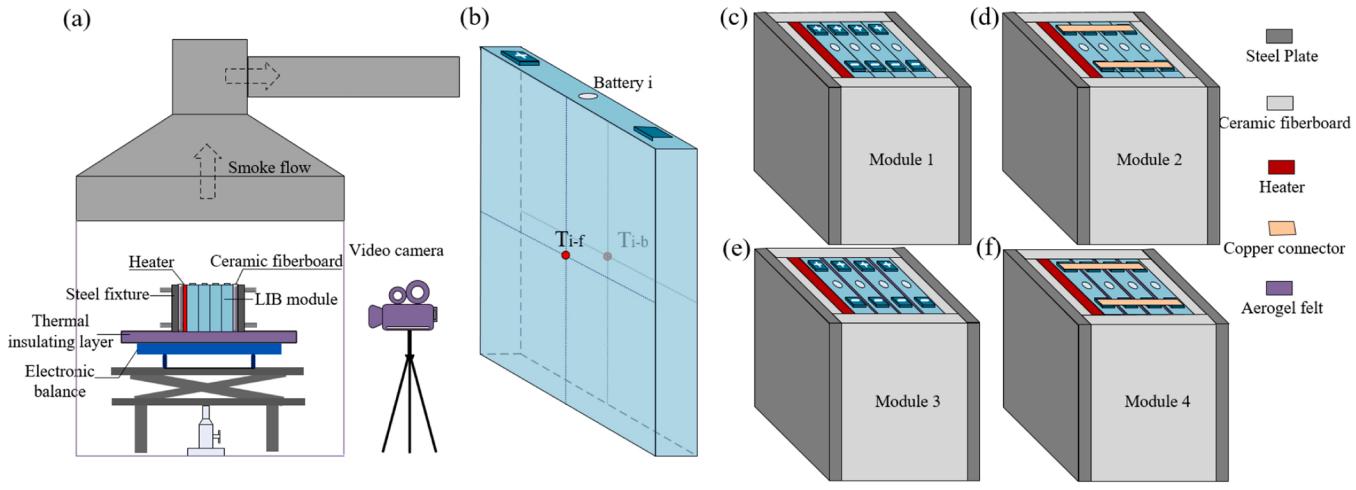

Fig. 1. Schematic diagram for experimental set up: (a) the experimental platform of TR propagation tests; (b) the thermocouple layout of each battery within the battery module; (c) the battery module without connection and prevention; (d) the battery module in parallel but without prevention; (e) the battery module without connection but with prevention; (f) the battery in parallel and with prevention.

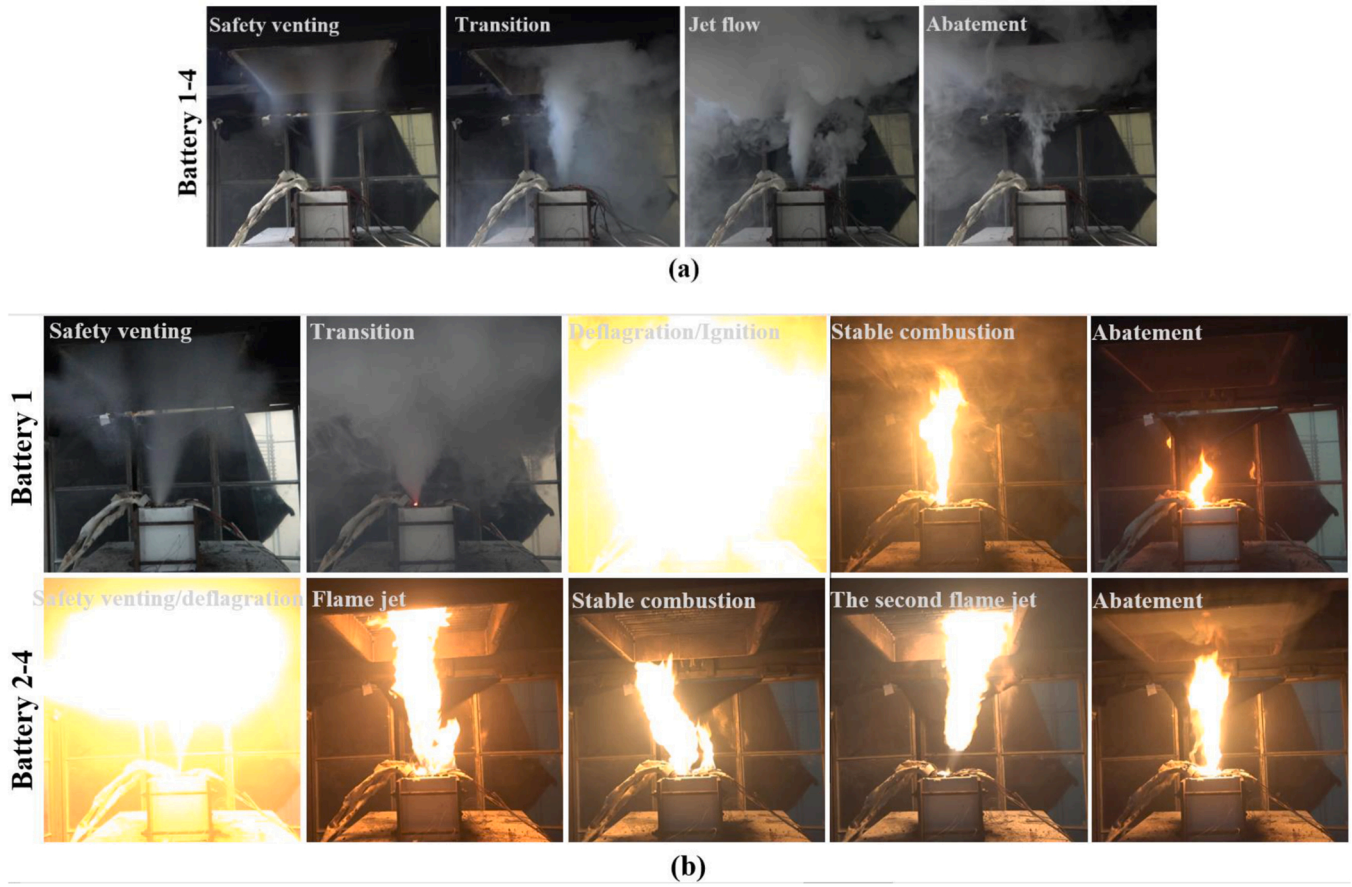

Fig. 2. Images of the TR propagation processes with different connections: (a) images for the module without connection; (b) images for the module in parallel.

battery 1 is similar to that of batteries within the module without connection, whereas a red dot can be observed in the pole of battery 1 connected to the copper connector during the stage of transition. The red dot may be attributed to the increase in temperature of the pole caused by the passage of the high current. At the late stage of TR, the ejected flammable gases and electrolyte vapors are ignited immediately by the red dot with high temperature, accompanied by a deflagration. After that, a stable combustion lasts for dozens of seconds and then begins to abate. In terms of battery 2–4, a large amount of gases and vapors are ignited immediately by the feeble flame of the former battery at the moment of safety venting, resulting in a deflagration. After safety venting, a jet flame can be observed, which lasts for several seconds, then transitions into stable combustion. Once TR is triggered, the battery emits a violent jet flame (higher than 60 cm in height), which is stronger and severer than the first one. It is interesting that the root of the second jet flame does not combust and phenomena of blow out can be observed due to the large jet velocity at the safety vent. After the second jet flame, the fire begins to slow and abate.

3.1.2. TR propagation features of batteries with different connections

The temperature and voltage responses of each battery within module 1 and 2 are illustrated in Fig. 3. As can be seen from Fig. 3(a)-(b), the steep temperature rise that corresponds to the incident of TR occurs on the front and back surfaces of each battery in modules sequentially. And a time interval between the onsets of TR for the battery front and back surfaces can be observed, which is attributed to the heat transfer in the direction of the battery thickness. In views of module 1, it can be seen that the voltage of each battery experiences a slight drop before safety venting due to the lithium-ion deintercalated from anode at high temperature. At the moment of safety venting, and the voltage suffers from a steeper decrease, which is corresponding to the micro internal short circuit. Once TR occurs inside the battery, the voltage drops sharply to 0 V because of the separator shrinks and the occurrence of the fierce internal short circuit. In contrast to the voltage response of the module 1, the voltage variations of each battery in module 2 are consistent due to parallel. The voltage drops firstly and then rises during TR of each battery, and it drops steeply to 0 V when the last battery in module 2 experiences TR, which is shown in Fig. 3(b). Furthermore, the time of overall TR propagation in module 1 and 2 are 2216 s and 1131 s, which demonstrates that the connection of parallel promotes the speed of TR propagation in the battery module. In order to capture more specific information about TR propagation time, each TR propagation time between two adjacent batteries for module 1 and 2 are summarized in Fig. 3(c). It can be seen that the TR propagation times of module 1 are all higher than that of module 2. Particularly, the TR propagation time between battery 3 and 4 is lower than others, which is because the heat accumulation in the module accelerates TR propagation.

For the battery module 1 and 2, the temperatures of battery 1–3 all experience two peaks. For example, the heat release during TR of battery 1 brings the temperature to the first peak. Once TR of battery 2 is induced, the partial heat will transfer from battery 2 to battery 1, causing the temperature of battery 1 to reach the second peak. The maximum temperature of the battery during TR propagation can be expressed through Eq. (1), and the results are summarized in Fig. 3(d). In module 1, the maximum temperatures of batteries 1–4 are 341.6 ℃, 335.5 ℃, 363.6 ℃ and 408.7 ℃, respectively, showing an increasing trend in maximum temperature as TR propagates in the battery module, which is attributed to the pre-heating effect. During TR propagation, the heat released from the TR battery transfers to other normal batteries, causing the subsequent batteries to suffer from higher initial temperatures in comparison with the previous batteries. The pre-heating effect results in an increase in maximum temperature as the propagation

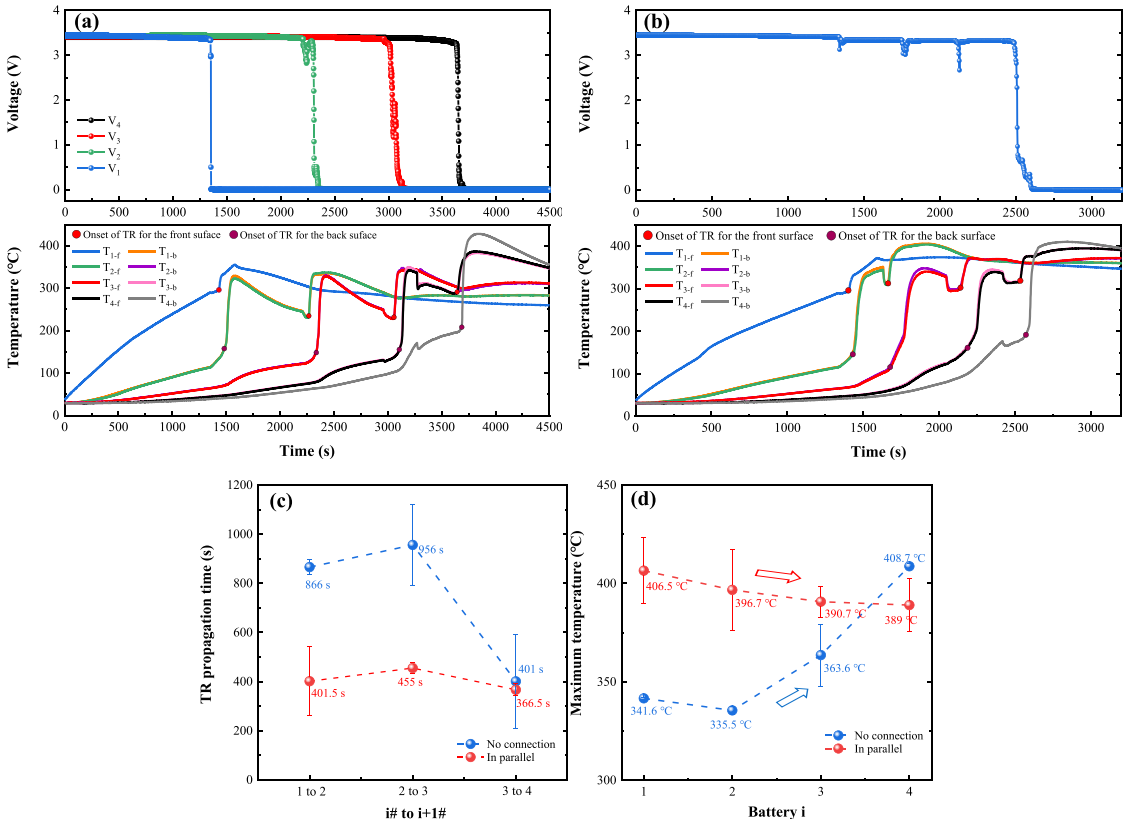

Fig. 3. The temperature and voltage responses during TR propagation without prevention: (a) variations of temperature and voltage for the module without connection (module 1); (b) variations of temperature and voltage for the module in parallel (module 2); (c) the TR propagation times between adjacent batteries within the module;*(d) the maximum temperature of battery i during TR propagation.*

proceeds due to the same heat release of each TR battery. However, the maximum temperatures in module 2 are 406.5 ℃, 396.7 ℃, 390.7 ℃ and 389 ℃ for battery 1–4, which exhibits a decreasing tendency. The root cause of the decrease tendency in maximum temperature for module 2 can be attributed to the transfer of electric current (Gao et al., 2019; Xu et al., 2021a), which is illustrated in Fig. 4. Once TR occurs in battery 1, the electric current will be transferred from the other three normal batteries to the battery 1 due to a voltage difference between the parallel-connected batteries and the TR battery, resulting in battery 1 releasing more energy than 100 % SOC state during TR. Since the electric energy of other batteries are transferred to battery 1, the SOCs of these battery are lower than 100 %. Similar situations occurs in other batteries as the TR propagation continues, causing the subsequent battery to release lower energy during TR compared to the former battery. Besides, all data for the TR propagation time and maximum temperature and of module 1 and 2 are listed in Supplementary Information.

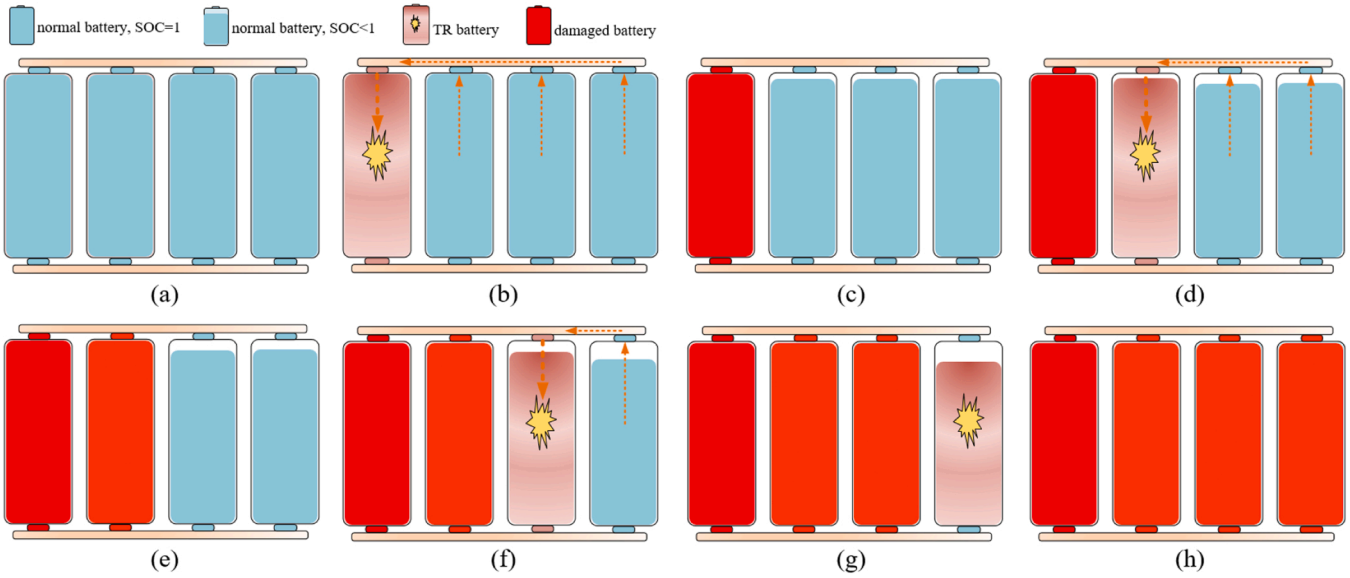

Fig. 4. Electrical processes of the module in parallel during TR propagation.

$$T_{max,i} = Max\left\{\frac{T_{i-f}(t) + T_{i-b}(t)}{2}\right\} \quad (1)$$

where $T_{max,i}$ is the maximum temperature of battery i, $T_{i-f}(t)$ and $T_{i-b}(t)$ are the temperatures of front and back surfaces at time t, respectively.

In addition to the temperature responses, Table 2 lists the mass losses of the two modules. For the LFP battery, the electrolyte and $LiFePO_4$ almost account for 14 % and 25 % for the total battery mass (Ping et al., 2015). And the mass losses of the electrolyte and $LiFePO_4$ are the primary mass loss of the TR battery. As listed in Table 2, the total mass losses of module 1 and 2 are almost the same. Each battery within the two modules owns an average mass loss in a value of 310 g, and a mass loss fraction of 22.3 %. It indicates that the losses of electrolyte and $LiFePO_4$ for the batteries experience TR is not influenced by the connection modes.

3.2. The effects on preventing TR propagation using aerogel

In view of prismatic batteries, the heat transferred through the battery shell dominates the heat sources for triggering TR of the adjacent battery during TR propagation (Feng et al., 2015b). Consequently, aerogel felts are selected to alleviate TR propagation in the battery modules with different connections. Fig. 5 presents the temperature and voltage responses of the modules without/with connectors under the passive prevention. It is worth noting that TR propagations of the two modules are both completely prevented by increasing the thermal resistance between adjacent batteries, and no incidents of safety venting (SV) and TR occur in battery 2–4, as shown in Fig. 5(a)-(b). Interestingly, the temperature variations of module 4 are similar to that of module 3, demonstrating that aerogel felts have significant effects on preventing TR propagation of battery modules with and without connectors. The peak temperatures for front and back surfaces of battery 2 in module 3 are 168.2 ℃ and 138.8 ℃, and in module 4 are 169.7 ℃ and 141 ℃, which are lower than the temperature of safety venting. Furthermore, as shown in Fig. 5(a), the voltage of battery 2 in module 3 drops from 3.43 V to 3.35 V slowly because of the lithium-ion deintercalated from anode at high temperature, and the voltages of subsequent batteries remain constant. As shown in Fig. 5(b), a voltage wave for module 4 can be observed after TR of battery 1 is triggered, and the voltage decrease from the initial 3.43 V to the final 3.33 V due to the transfer of electric current.

The maximum temperatures of each battery in the two modules are captured based on Eq. (1), as presented in Fig. 5(c). Since TR propagation within the modules is successfully prevented, the maximum temperatures of subsequent batteries are all lower than 200 ℃. For module 4, the maximum temperatures of battery 2–4 are 162.8 ℃, 101 ℃ and 82.1 ℃, which are higher than that of module 3. This can be attributed to the fact that part of the heat released by battery 1 is transferred to other batteries through the copper connectors. In addition, the first peak temperatures of battery 1 during its TR in different battery modules are compared, as shown in Table 3. For comparison, the first peak temperatures of battery 1 before battery 2 experiencing TR in module 1 and 2 are captured. It can be seen that the temperature of battery 1 with prevention is higher than that of battery 1 without prevention, which is attributed to the excellent thermal insulation performance of aerogel. During TR of battery 1 in the modules with prevention, the heat transfer from battery 1 to subsequent batteries is reduced by the aerogel, causing more heat is used to raise the temperature of battery 1.

Furthermore, an equivalent circuit model (Gao et al., 2019) is established to quantitatively describe the transferred electricity for the module in parallel under passive prevention (module 4), as shown in Fig. 6. During the TR stage of battery 1, the transfer capacity of electricity from other batteries and the energy of transferred electricity can be determined by Eqs. (2)–(5). As listed in Table 3, battery 1 has 103.65 % SOC during TR, and 1.83 Ah capacity of electricity is transferred from other batteries to battery 1, leading to 22.43 kJ electric energy transferred during the transfer of electric current. Based on Eq. (6), the contribution of the electric energy transferred to the increase in the battery temperature can be obtained. The increase in temperature due to the electrical transfer is calculated to be 14.6 ℃. This demonstrates that the transferred electricity for the module in parallel has no significant influence on the energy release of the TR battery. Besides, Table 4 compares the transferred electricity and electric energy from this study and other investigations. For the batteries in parallel, the electricity transfer from subsequent batteries to the battery 1 accounts for approximately 3 % of the total battery capacity during TR propagation, which demonstrates that the capacity of transferred electricity is small in comparison with the capacity of 100 % SOC battery.

$$V = E - IR_b \quad (2)$$

$$R_{TR} = \frac{V}{IN} \quad (3)$$

$$Q_e = \int_{t_0}^{t_1} INdt \quad (4)$$

$$H_e = Q_e \times V \times 3600 \quad (5)$$

$$H_e = m_b c_b \Delta T \quad (6)$$

where V is the terminal voltage of the battery module, E is the electric potential of normal cell, I is the current transferred from normal battery to the battery in TR, R_b is the resistance of normal battery (the resistance of the battery is 0.7 mΩ), R_{TR} is the resistance of TR battery, N is the number of normal batteries, Q_e is the transfer capacity of electricity from other batteries, t_0 and t_1 are the start and end times of charging battery 1, H_e is the energy of transferred electricity, m_b is the battery mass, c_b is the specific heat capacity of the tested battery (the value of c_b is about 1.1 J/g•K).

3.3. Heat transfer analysis for different battery modules

The transferred heat flow in the battery thickness direction is the root cause of TR propagation within the module made of prismatic batteries. Identifying the total heat absorbed by the battery before its TR is of great significance to reveal TR propagation mechanisms with different connections. Under thermal abuse conditions, the battery not only absorbs the external heat but also generates heat at elevated temperature owing to exothermic reactions. The heat generation of the battery is assumed to be comprised of the heat from solid electrolyte interface (SEI) decomposition, the heat from the reaction between anode and electrolyte, the heat from the reaction between cathode and electrolyte, the heat from the electrolyte decomposition, and the joule heat of internal short circuit (Zhang et al., 2021). Due to the complexity of heat sources during TR, the self-generated heat of the battery (Q_{self}) is used to represents the all heat generated inside the battery. In order to determine the heat absorbed by the battery before TR (Q_b), it is necessary to obtain the self-generated heat of the battery. Consequently, the experiments about the normal and failure batteries are conducted to identify the self-generated heat of the battery before TR, and the experimental schematic diagram is displayed in Fig. 7(a). The normal battery is heated by the heater with 500 W heating power to determine the internal heat

Table 2
The mass loss data.

Connection type	Total mass loss (g)	Average mass loss of per battery (g)	Mass loss fraction (%)
No connection	1243.15±25.65	310.79±6.41	22.28±0.46
In parallel	1247.15±12.95	311.79±3.24	22.35±0.23

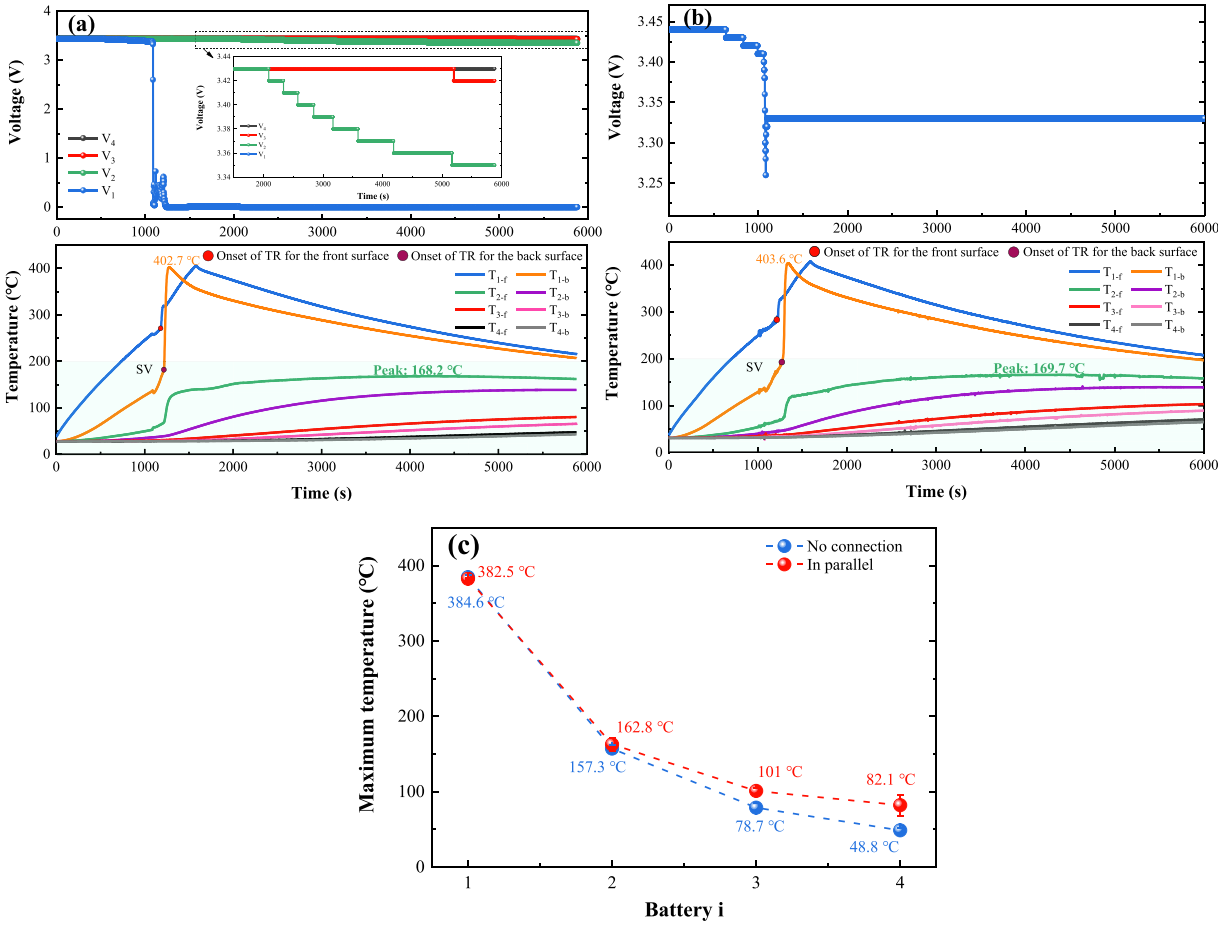

Fig. 5. The temperature and voltage responses during TR propagation with passive prevention: (a) variations of temperature and voltage for the module without connection (module 3); (b) variations of temperature and voltage for the module in parallel (module 4); (c) the maximum temperature of battery i during TR propagation.

Table 3
Comparison of the peak temperature of battery 1 before battery 2 experiencing TR for different modules.

Connection	Passive prevention	First peak temperature (°C)
No connection	No	341.6±0.68
	Yes	384.6±3.15
In parallel	No	360.7±0.88
	Yes	382.5±1.33

increasing in the battery before TR. As expressed in Eq. (7), the heat sources that raise the temperature of the battery before TR are composed of the heat absorbed by the battery and the self-generated heat of the battery. The failure battery with zero energy storage is heated under the same experimental condition to identify the heat absorbed by the normal battery. Hence, the self-generated heat of the normal battery can be determined by Eqs. (7)–(8), which is reasonably assumed to be the same as the heat generated by the batteries within modules due to the same experimental conditions. Fig. 7(b) depicts the variations of internal heat increasing in the battery and the heat absorbed by the battery.

$$c_b m_b (T_b - T_\infty) = Q_b + Q_{self} \tag{7}$$

$$Q_b = c_b' m_b' (T_b' - T_\infty) \tag{8}$$

where Q_b and Q_{self} are the heat absorbed by the battery and the self-generated heat of the battery before TR, respectively, c_b' is the specific heat capacity of the failure battery (which is assumed be the same as c_b),

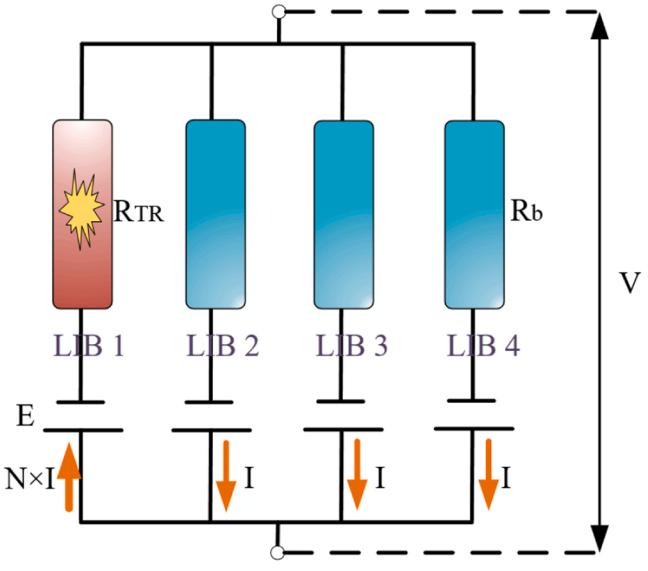

Fig. 6. The equivalent circuit model for the module 4 in parallel.

m_b' is the mass of the failure battery, T_b and T_∞ are the average temperature of the normal battery and the ambient temperature, respectively, and T_b' is the average temperature of the failure battery.

Table 4
Comparison of electricity and electric energy transfer to battery 1 of LIB module from this study and other studies.

Ref.	Capacity (Ah)	SOC (%)	Transfer electricity (Ah)	Transfer electric energy (kJ)
This study	50	103.65±0.44	1.83±0.22	22.43±2.7
(Gao et al., 2019)	24	103.42	0.82	12.31
(Xu et al., 2021a)	31.6	103.4	1.07	16.06

$$Q_{i,\ b} = c_b m_b\left(T_{onset,i} - T_\infty\right) - Q_{self}\left(T_{onset,i}\right) \quad (9)$$

where $Q_{i,b}$ is the heat absorbed by battery i before its TR, $T_{onset,i}$ is the onset temperature of TR for battery i, $Q_{self}(T_{onset,i})$ is the self-generated heat of battery i at $T_{onset,i}$.

As for the battery modules without passive prevention, the heat absorbed by each battery before TR can be identified by Eq. (9). In addition, the contributions of the heat transferred from previous batteries to induce TR of subsequent batteries can be clarified based on Eq. (10), and the contributions of the heat transferred from the heater to trigger TR of the battery within the module is determined by Eq. (11). It should be noted that the heat absorbed by battery 1 comes from the

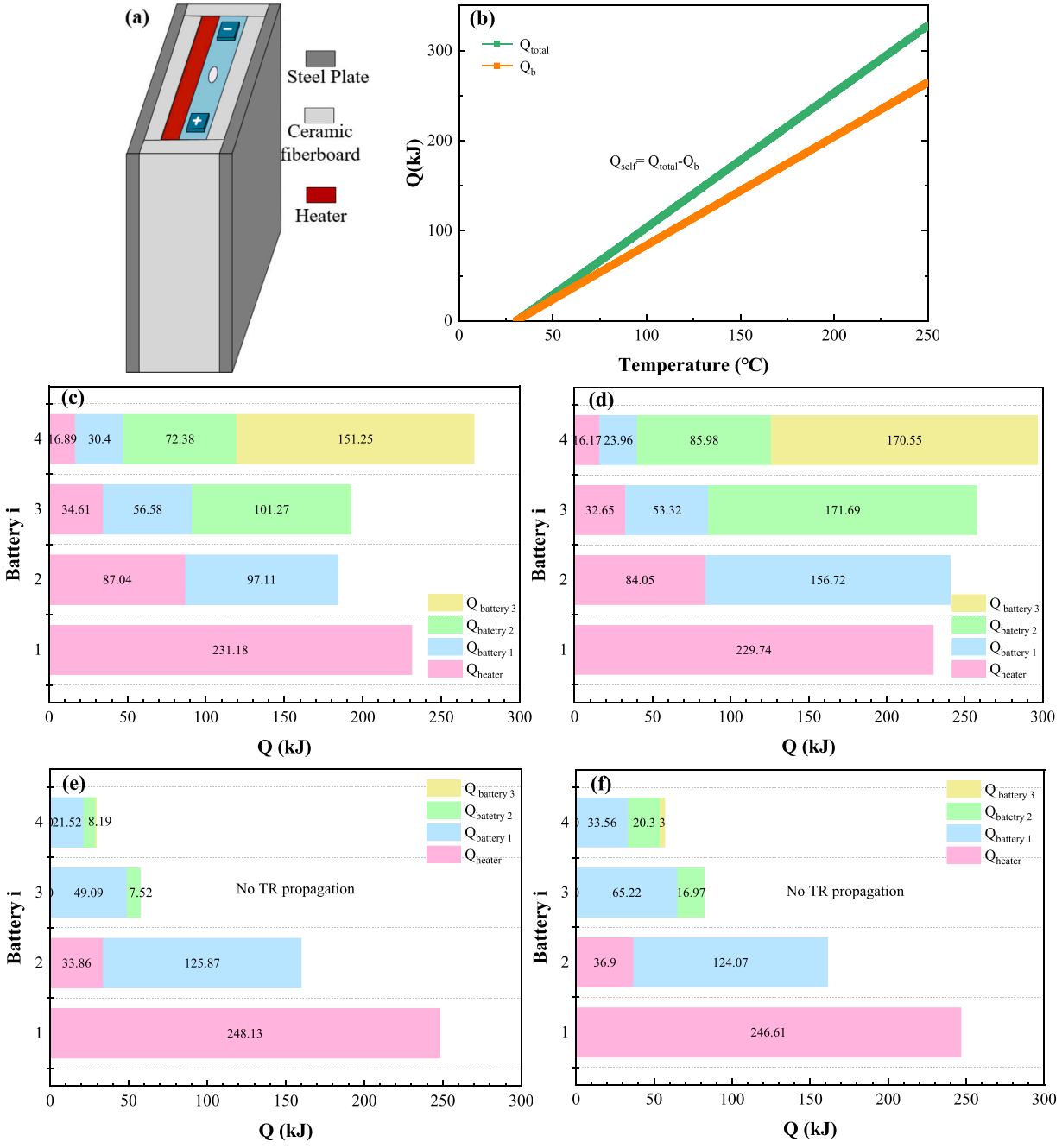

Fig. 7. Calculation of absorbed heats during TR propagation for different modules: (a) Schematic diagram of the overheating experiments for determining the self-generated heat of the battery before TR; (b) the absorbed heat varieties with temperature for the fresh battery and the failure battery; (c) the heat absorbed by battery i during TR propagation for module 1; (c) the heat absorbed by battery i during TR propagation for module 2; (d) the heat absorbed by battery i during TR propagation for module 3; (f) the heat absorbed by battery i during TR propagation for module 4.

heater, and the heat absorbed by other batteries comes from previous batteries experienced TR and the heater.

$$Q_{b-j,i} = c_b m_b\left(T_{b,i}(t_{onset,j+1}) - T_{b,i}(t_{onset,j})\right) - Q_{self,t_{onset,j}-t_{onset,j+1}}, \quad (i > j) \tag{10}$$

$$Q_{heater,i} = \left\{ \begin{array}{c} Q_{i,b} \quad (i=1) \\ Q_{i,b} - \sum_{j=1}^{i-1} Q_{i,b-j} \quad (i>1, \&\&i>j\&\&\&\&) \end{array} \right\} \tag{11}$$

where $Q_{b-j,i}$ is the contribution of the heat generated from battery j to induce the TR of battery i, $t_{onset,j}$ and $t_{onset,j+1}$ represent the onset times of TR for battery j and battery j + 1, $T_{b,i}(t_{onset,j})$ represents the average temperature of battery i at the moment of $t_{onset,j}$ and $T_{b,i}(t_{onset,j+1})$ represents the average temperature of battery i at the moment of $t_{onset,j+1}$, $Q_{self,t_{onset,j}-t_{onset,j+1}}$ represents the self-generated heat of battery i between the time interval of $t_{onset,j}$ and $t_{onset,j+1}$, $Q_{heater,i}$ is the contributions of the heat transferred from the heater to trigger TR of battery i.

Owing to the excellent performance of aerogel on preventing TR propagation, no TR occurs in subsequent batteries after TR of battery 1 is induced for the modules with prevention. Hence, the time nodes corresponding to the maximum temperatures of battery 2–4 are selected to determine the total heat absorbed by each battery ($Q_{i,b}$) in the modules and clarify contributions of the heat from previous batteries ($Q_{i,b-j}$) to subsequent batteries, as expressed in Eqs. (12)-(13). Additionally, the contributions of the heat from the heater to each battery within the modules can be determined by Eq. (11).

$$Q_{b,i} = \left\{ \begin{array}{l} c_b m_b\left(T_{onset,i} - T_\infty\right) - Q_{self}\left(T_{onset,i}\right) \quad (i=1) \\ c_b m_b\left(T_{max,i} - T_\infty\right) - Q_{self}\left(T_{max,i}\right) \quad (i>1) \end{array} \right\} \tag{12}$$

$$Q_{b-j,i} = \left\{ \begin{array}{l} c_b m_b\left(T_{b,i}(t_{max,j+1}) - T_{b,i}(t_{onset,j})\right) - Q_{self,t_{onset,j}-t_{max,j+1}} \quad (i>j\&, j=1) \\ c_b m_b\left(T_{b,i}(t_{max,j+1}) - T_{b,i}(t_{max,j})\right) - Q_{self,t_{max,j}-t_{max,j+1}} \quad (i>j, j>1) \end{array} \right\} \tag{13}$$

where $T_{max,i}$ represents the maximum temperature of battery i, $t_{max,j}$ and $t_{max,j+1}$ represent the moments of reaching maximum temperature for battery j and battery j + 1, $T_{b,i}(t_{max,j})$ represents the temperature of battery i at the moment of $t_{max,j}$, and $T_{b,i}(t_{max,j+1})$ represents the temperature of battery i at the moment of $t_{max,j+1}$, $Q_{self,t_{onset,j}-t_{max,j+1}}$ represents the self-generated heat of battery i between the time interval of $t_{onset,j}$ and $t_{max,j+1}$, $Q_{self,t_{max,j}-t_{max,j+1}}$ represents the self-generated heat of battery i between the time interval of $t_{max,j}$ and $t_{max,j+1}$.

Based on the above analysis, Fig. 7(c)-(f) illustrate the transferred heat flows during TR propagation for different modules. As shown in Fig. 7(c)-(d), the heat from the battery suffered from TR is the dominant heat source for triggering TR of the adjacent battery, which contributes to 52 %−67 % of the total heat absorbed. And the contributions of other batteries experienced TR to trigger the TR of the subsequent battery cannot be ignored. It should be noted that 184 kJ is sufficient to trigger TR of the battery and lead to TR propagation within the battery module. In addition, the total heat absorbed by the subsequent battery before TR increases as TR propagation continues, which may be attributed to the heat accumulation within the modules. Compared with the module without connection, the batteries of the module in parallel absorb more heat before TR.

Fig. 7(e)-(f) depicts the transferred heat flows during TR propagation for the modules with prevention. Compared with the modules without prevention, the heat absorbed by subsequent batteries within module 3 and 4 is much lower, which demonstrates that TR propagation can be prevented once the heat absorbed by the battery is reduced. It can be seen that the heat of battery 1 generated at TR stage is responsible for the temperature increase of other batteries, and the heat from the batteries without experiencing TR has little impact on TR propagation. Interestingly, the transferred heat during TR propagation of module 3 is similar to that of module 4 due to the application of aerogel, showing that the aerogel has same effects on reducing the transfer heat and preventing TR propagation for the modules with different connections.

For the module in parallel, the heat generated in TR spreads to the adjacent battery mainly through the shell, connectors and flame radiation, as shown in Fig. 8(a). Owing to no connectors and flame for the module without connection, the shell is the main path of the heat transfer. As shown in Fig. 7(e)-(f), the heat absorbed by battery 2 is about 160 kJ for module 3 and 4, demonstrating that the heat that the battery shell is the main path of the heat transfer during TR propagation for the modules with different connections. The result also reveals that the flame and the connectors have little influence on TR propagation. Enhancing thermal resistances between adjacent batteries is the most effective method to prevent TR propagation in terms of prismatic battery modules.

Furthermore, the average heat fluxes of the former battery to its adjacent battery for the modules without prevention are calculated by Eq. (14), and the average heat flux for the modules with prevention are calculated by Eq. (15). As shown in Fig. 8(b), the heat flux of the former battery to the neighboring battery are about 400 W for the module in parallel, which are much higher than those of the module without connection, especially in the early stage of TR propagation. Consequently, the TR propagation speed within the parallel module is much faster in comparison with the module without connection. Fig. 8(c) presents the average heat flux of the modules with prevention. It can be seen that heat flux of module 3 and 4 are almost consistent, and the average heat flux from battery 1 that experienced TR to battery 2 is about 35 W, indicating the aerogel with low thermal conductivity has excellent performances in reducing heat flux for the modules. By comparing the module 1–4, the module 3 and 4 have similar thermal responses owing to the reduction of the heat flux. Particularly, the parallel connection aggravates exothermic reactions inside the battery during TR, resulting in high heat flux of the battery to its adjacent battery, which is the main cause of the battery module in parallel with fiercer TR propagation. It should be noted that increasing thermal resistances between adjacent batteries is an effective method to reduce the risk of module in parallel and prevent TR propagation.

$$P_{ave} = \frac{Q_{b-i,i+1}}{t_{onset,i+1} - t_{onset,i}} \tag{14}$$

$$P_{ave} = \left\{ \begin{array}{l} \frac{Q_{b-i,i+1}}{t_{max,i+1} - t_{onset,i}} \quad (i=1) \\ \frac{Q_{b-i,i+1}}{t_{max,i+1} - t_{max,i}} \quad (i>1) \end{array} \right\} \tag{15}$$

where P_{ave} is the average heat flux of the battery to the adjacent battery during TR propagation, $Q_{b-i,i+1}$ is the heat transfer from battery i to battery i + 1, $t_{onset,i+1}$ is the onset time of TR for battery i, $t_{max,i}$ is the moment of reaching the maximum temperature for battery i.

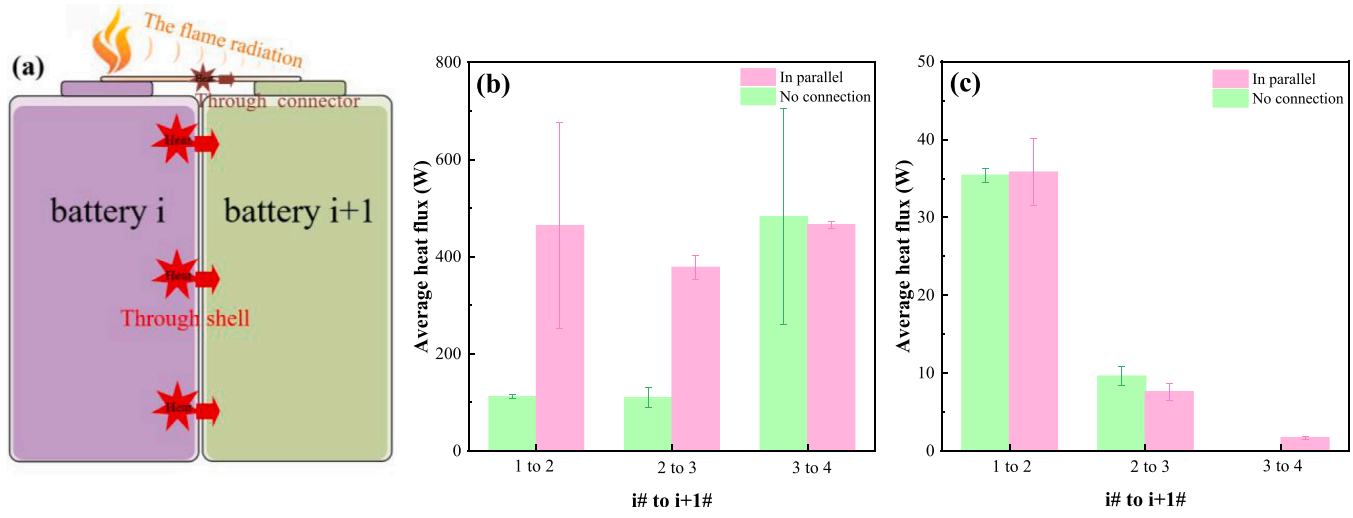

Fig. 8. The average heat flux of the former battery to its adjacent battery during TR propagation: (a) the heat transfer paths from the former battery to its adjacent battery during TR; (b) the average heat flux of battery i to battery i + 1 for the modules without prevention; (c) the average heat flux of the battery i to battery i + 1 for the modules with passive prevention.

4. Conclusions

In this study, the TR propagation characteristics of the battery modules with different connections and the performances of aerogel on preventing TR propagation for these battery modules are experimentally investigated. The TR propagation mechanisms of the modules are also revealed in term of the transfer heat in the direction of the battery thickness. The contributions of the heat transferred from previous batteries to induce TR of subsequent batteries are clarified for the first time, and the dominated heat transfer path during TR propagation is identified. The main conclusions of this study are summarized as follows:

(1) During TR propagation, violent jet flames can be observed in the battery module in parallel, whereas no any combustion occurs in the battery module without connection. Owing to the transferred electricity, the maximum temperature in the parallel batteries decreases with the continuation of TR propagation, which is contrary to the result of the battery module without connection.

(2) The heat from the battery suffered from TR is the primary heat source for triggering TR of the adjacent battery (contributes to 52 %−67 %), whereas the heat from other batteries for triggering the TR cannot be ignored. The average heat flux energy during TR propagation is about 400 W for the battery module in parallel, which is much higher than that of the battery module without connection.

(3) The transferred electricity can only increase the temperature of TR battery by 16 ℃, which has no significant impact on the energy released during TR propagation. While the parallel connection mode intensifies the thermochemical reactions inside the battery accompanied with high heat flux energy releasing, leading to more violent combustion and shorter TR propagation time in comparison with other electrical connection modes.

(4) TR propagation in the battery modules with different connections can be completely prevented by adopting aerogel. The average heat flux of the former battery to its adjacent battery can be reduced from 400 W to 35 W by using aerogel. During TR propagation of the battery module in parallel, the thermal conduction between battery shells is the dominant heat transfer path during TR propagation, and the heat transfer through connectors or flame radiation has little influence on TR propagation. Enhancing thermal resistances between adjacent batteries is an effective method to prevent TR propagation for the battery module in parallel.

In brief, the findings provide new insights into the cause of fiercer TR propagation within the battery module in parallel and enhance the understanding of TR propagation behaviors. Besides, the excellent performances of the thermal insulation in preventing TR propagation of the battery module in parallel are experimentally verified, holding enormous promise for the safer battery modules.

Declaration of Competing Interest

The authors declare that they have no known competing financial interests or personal relationships that could have appeared to influence the work reported in this paper.

Acknowledgments

This work was supported by the Fundamental Research Funds for the Central Universities under Grant No. WK2320000053, and the Research Grants Council of the Hong Kong Special Administrative Region, China (Project No. 9043135, CityU 11202721).

Appendix A. Supporting information

Supplementary data associated with this article can be found in the online version at doi:10.1016/j.psep.2022.06.048.

References

Chen, M., Dongxu, O., Liu, J., Wang, J., 2019. Investigation on thermal and fire propagation behaviors of multiple lithium-ion batteries within the package. Appl. Therm. Eng. 157, 113750.

Chen, M., Liu, J., Ouyang, D., Weng, J., Wu, X., Cao, S., Wang, J., 2020. A large-scale experimental study on the thermal failure propagation behaviors of primary lithium batteries. J. Energy Storage 31, 101657.

Duh, Y.-S., Theng, J.-H., Chen, C.-C., Kao, C.-S., 2020. Comparative study on thermal runaway of commercial 14500, 18650 and 26650 LiFePO4 batteries used in electric vehicles. J. Energy Storage 31, 101580.

Feng, X., He, X., Ouyang, M., Lu, L., Wu, P., Kulp, C., Prasser, S., 2015a. Thermal runaway propagation model for designing a safer battery pack with 25 Ah LiNi Co Mn O2 large format lithium ion battery. Appl. Energy 154, 74–91.

Feng, X., Ren, D., He, X., Ouyang, M., 2020. Mitigating thermal runaway of lithium-ion batteries. Joule 4, 743–770.

Feng, X., Sun, J., Ouyang, M., Wang, F., He, X., Lu, L., Peng, H., 2015b. Characterization of penetration induced thermal runaway propagation process within a large format lithium ion battery module. J. Power Sources 275, 261–273.

Feng, X., Zheng, S., Ren, D., He, X., Wang, L., Cui, H., Liu, X., Jin, C., Zhang, F., Xu, C., Hsu, H., Gao, S., Chen, T., Li, Y., Wang, T., Wang, H., Li, M., Ouyang, M., 2019. Investigating the thermal runaway mechanisms of lithium-ion batteries based on thermal analysis database. Appl. Energy 246, 53–64.

Gao, S., Feng, X., Lu, L., Kamyab, N., Du, J., Coman, P., White, R.E., Ouyang, M., 2019. An experimental and analytical study of thermal runaway propagation in a large format lithium ion battery module with NCM pouch-cells in parallel. Int. J. Heat. Mass Transf. 135, 93–103.

Huang, P., Ping, P., Li, K., Chen, H., Wang, Q., Wen, J., Sun, J., 2016. Experimental and modeling analysis of thermal runaway propagation over the large format energy storage battery module with Li4Ti5O12 anode. Appl. Energy 183, 659–673.
Huang, Z., Li, X., Wang, Q., Duan, Q., Li, Y., Li, L., Wang, Q., 2021a. Experimental investigation on thermal runaway propagation of large format lithium ion battery modules with two cathodes. Int. J. Heat Mass Transf. 172, 121077.
Huang, Z., Liu, J., Zhai, H., Wang, Q., 2021b. Experimental investigation on the characteristics of thermal runaway and its propagation of large-format lithium ion batteries under overcharging and overheating conditions. Energy 233, 121103.
Huang, Z., Zhao, C., Li, H., Peng, W., Zhang, Z., Wang, Q., 2020. Experimental study on thermal runaway and its propagation in the large format lithium ion battery module with two electrical connection modes. Energy 205, 117906.
Kriston, A., Kersys, A., Antonelli, A., Ripplinger, S., Holmstrom, S., Trischler, S., Döring, H., Pfrang, A., 2020. Initiation of thermal runaway in Lithium-ion cells by inductive heating. J. Power Sources 454, 227914.
Lamb, J., Orendorff, C.J., Steele, L.A.M., Spangler, S.W., 2015. Failure propagation in multi-cell lithium ion batteries. J. Power Sources 283, 517–523.
Larsson, F., Bertilsson, S., Furlani, M., Albinsson, I., Mellander, B.-E., 2018. Gas explosions and thermal runaways during external heating abuse of commercial lithium-ion graphite-LiCoO2 cells at different levels of ageing. J. Power Sources 373, 220–231.
Lee, C., Said, A.O., Stoliarov, S.I., 2020. Passive mitigation of thermal runaway propagation in dense 18650 lithium ion cell assemblies. J. Electrochem. Soc. 167, 090524.
Li, L., Xu, C., Chang, R., Yang, C., Jia, C., Wang, L., Song, J., Li, Z., Zhang, F., Fang, B., Wei, X., Wang, H., Wu, Q., Chen, Z., He, X., Feng, X., Wu, H., Ouyang, M., 2021. Thermal-responsive, super-strong, ultrathin firewalls for quenching thermal runaway in high-energy battery modules. Energy Storage Mater. 40, 329–336.
Li, M., Lu, J., Chen, Z., Amine, K., 2018. 30 years of lithium-ion batteries. Adv. Mater., e1800561
Lisbona, D., Snee, T., 2011. A review of hazards associated with primary lithium and lithium-ion batteries. Process Saf. Environ. Prot. 89, 434–442.
Liu, T., Tao, C., Wang, X., 2020. Cooling control effect of water mist on thermal runaway propagation in lithium ion battery modules. Appl. Energy 267, 115087.
Lyon, R.E., Walters, R.N., 2016. Energetics of lithium ion battery failure. J. Hazard Mater. 318, 164–172.
Ma, R., Du, P., Li, T., 2021. Climate change, environmental factors, and COVID-19: Current evidence and urgent actions. Innovation 2, 100138.
Mao, B., Chen, H., Jiang, L., Zhao, C., Sun, J., Wang, Q., 2020. Refined study on lithium ion battery combustion in open space and a combustion chamber. Process Saf. Environ. Prot. 139, 133–146.
Niu, H., Chen, C., Liu, Y., Li, L., Li, Z., Ji, D., Huang, X., 2022. Mitigating thermal runaway propagation of NCM 811 prismatic batteries via hollow glass microspheres plates. Process Saf. Environ. Prot. 162, 672–683.
Niu, X., Garg, A., Goyal, A., Simeone, A., Bao, N., Zhang, J., Peng, X., 2019. A coupled electrochemical-mechanical performance evaluation for safety design of lithium-ion batteries in electric vehicles: an integrated cell and system level approach. J. Clean. Prod. 222, 633–645.
Ping, P., Kong, D., Zhang, J., Wen, R., Wen, J., 2018. Characterization of behaviour and hazards of fire and deflagration for high-energy Li-ion cells by over-heating. J. Power Sources 398, 55–66.
Ping, P., Wang, Q., Huang, P., Li, K., Sun, J., Kong, D., Chen, C., 2015. Study of the fire behavior of high-energy lithium-ion batteries with full-scale burning test. J. Power Sources 285, 80–89.
Qin, P., Jia, Z., Jin, K., Duan, Q., Sun, J., Wang, Q., 2021. The experimental study on a novel integrated system with thermal management and rapid cooling for battery pack based on C6F12O spray cooling in a closed-loop. J. Power Sources 516, 230659.
Rogelj, J., den Elzen, M., Hohne, N., Fransen, T., Fekete, H., Winkler, H., Schaeffer, R., Sha, F., Riahi, K., Meinshausen, M., 2016. Paris agreement climate proposals need a boost to keep warming well below 2 degrees C. Nature 534, 631–639.
Said, A.O., Garber, A., Peng, Y., Stoliarov, S.I., 2021. Experimental investigation of suppression of 18650 lithium ion cell array fires with water mist. Fire Technol. 58, 523–551.
Said, A.O., Lee, C., Stoliarov, S.I., 2020. Experimental investigation of cascading failure in 18650 lithium ion cell arrays: Impact of cathode chemistry. J. Power Sources 446, 227347.
Said, A.O., Lee, C., Stoliarov, S.I., Marshall, A.W., 2019. Comprehensive analysis of dynamics and hazards associated with cascading failure in 18650 lithium ion cell arrays. Appl. Energy 248, 415–428.
Wang, Q., Mao, B., Stoliarov, S.I., Sun, J., 2019. A review of lithium ion battery failure mechanisms and fire prevention strategies. Prog. Energy Combust. Sci. 73, 95–131.
Wilke, S., Schweitzer, B., Khateeb, S., Al-Hallaj, S., 2017. Preventing thermal runaway propagation in lithium ion battery packs using a phase change composite material: an experimental study. J. Power Sources 340, 51–59.
Wu, S., Li, T., Wu, M., Xu, J., Hu, Y., Chao, J., Yan, T., Wang, R., 2020. Highly thermally conductive and flexible phase change composites enabled by polymer/graphite nanoplatelet-based dual networks for efficient thermal management. J. Mater. Chem. A 8, 20011–20020.
Xu, C., Zhang, F., Feng, X., Jiang, F., Ren, D., Lu, L., Yang, Y., Liu, G., Han, X., Friess, B., Ouyang, M., 2021a. Experimental study on thermal runaway propagation of lithium-ion battery modules with different parallel-series hybrid connections. J. Clean. Prod. 284, 124749.
Xu, J., Duan, Q., Zhang, L., Liu, Y., Zhao, C., Wang, Q., 2021b. Experimental study of the cooling effect of water mist on 18650 lithium-ion battery at different initial temperatures. Process Saf. Environ. Prot.
Xu, X., Mi, J., Fan, M., Yang, K., Wang, H., Liu, J., Yan, H., 2019. Study on the performance evaluation and echelon utilization of retired LiFePO4 power battery for smart grid. J. Clean. Prod. 213, 1080–1086.
Yang, X., Duan, Y., Feng, X., Chen, T., Xu, C., Rui, X., Ouyang, M., Lu, L., Han, X., Ren, D., Zhang, Z., Li, C., Gao, S., 2020. An experimental study on preventing thermal runaway propagation in lithium-ion battery module using aerogel and liquid cooling plate together. Fire Technol. 56, 2579–2602.
Yuan, C., Wang, Q., Wang, Y., Zhao, Y., 2019. Inhibition effect of different interstitial materials on thermal runaway propagation in the cylindrical lithium-ion battery module. Appl. Therm. Eng. 153, 39–50.
Yuan, L., Dubaniewicz, T., Zlochower, I., Thomas, R., Rayyan, N., 2020. Experimental study on thermal runaway and vented gases of lithium-ion cells. Process Saf. Environ. Prot. 144, 186–192.
Zhang, Y., Mei, W., Qin, P., Duan, Q., Wang, Q., 2021. Numerical modeling on thermal runaway triggered by local overheating for lithium iron phosphate battery. Appl. Therm. Eng. 192, 116928.
Zhao, J., Xue, F., Fu, Y., Cheng, Y., Yang, H., Lu, S., 2021. A comparative study on the thermal runaway inhibition of 18650 lithium-ion batteries by different fire extinguishing agents. iScience 24, 102854.
Zhong, G., Li, H., Wang, C., Xu, K., Wang, Q., 2018. Experimental analysis of thermal runaway propagation risk within 18650 lithium-ion battery modules. J. Electrochem. Soc. 165, A1925–A1934.
Zhou, Z., Ju, X., Zhou, X., Yang, L., Cao, B., 2022a. A comprehensive study on the impact of heating position on thermal runaway of prismatic lithium-ion batteries. J. Power Sources 520, 230919.
Zhou, Z., Wang, D., Peng, Y., Li, M., Wang, B., Cao, B., Yang, L., 2022b. Experimental study on the thermal management performance of phase change material module for the large format prismatic lithium-ion battery. Energy 238, 122081.
Zhou, Z., Zhou, X., Wang, D., Li, M., Wang, B., Yang, L., Cao, B., 2021. Experimental analysis of lengthwise/transversal thermal characteristics and jet flow of large-format prismatic lithium-ion battery. Appl. Therm. Eng. 195, 117244.